Korean J. Chem. Eng., 36(2), 191-196 (2019)
DOI: 10.1007/s11814-018-0186-6

pISSN: 0256-1115
eISSN: 1975-7220

Effects of Al^{3+} precipitation onto primitive amorphous Cu-Zn precipitate on methanol synthesis over $Cu/ZnO/Al_2O_3$ catalyst

Cheonwoo Jeong*,‡,‡, Jongha Park*,‡, Jinsung Kim*, Joon Hyun Baik, and Young-Woong Suh*,***,†**

*Department of Chemical Engineering, Hanyang University, Seoul 04763, Korea
**Energy Research Group, Research Institute of Industrial Science & Technology, Pohang 37673, Korea
***Research Institute of Industrial Science, Hanyang University, Seoul 04763, Korea
(*Received 20 June 2018 • accepted 3 November 2018*)

Abstract−The phase of Cu,Zn,Al precursors strongly affects the activity of their final catalysts. Herein, the Cu,Zn,Al precursor was prepared by precipitation of Al^{3+} onto primitive, amorphous Cu,Zn precipitate. This precursor turned out to be a phase mixture of zincian malachite and hydrotalcite in which the latter phase was less abundant compared to the co-precipitated precursor. The final catalyst derived from this precursor exhibited a little higher copper surface area and methanol synthesis activity than the co-precipitated counterpart. Therefore, the two precursor phases need to be mixed in an adequate proportion for the preparation of active $Cu/ZnO/Al_2O_3$ catalyst.

Keywords: Methanol Synthesis, $Cu/ZnO/Al_2O_3$, Sequential Precipitation, Precursor Phase

INTRODUCTION

Co-precipitation (CP) has been widely used for the preparation of multi-component catalyst systems composed of non-reducible and/or reducible metal oxides. The structure of co-precipitated materials varies by adjusting several precipitation variables [1-5]. Nevertheless, more emphasis should be placed on the ageing step because a primitive precipitate of generally amorphous nature is transformed into a crystalline structure via dissolution and re-precipitation [6]. The example studied intensively is the binary Cu,Zn system of Cu-rich close to the ratio Cu/Zn of 7 : 3 [7-10]. Behrens demonstrated that the crystallization of amorphous zincian georgeite into zincian malachite was accompanied by sudden pH drop, turbidity increase, and color change from blue to green at 65 min after the start of ageing [9].

This pH drop was also observed during ageing of Cu,Zn,Al precursors with the Al content of 2.5-13.0%, where constant pH co-precipitation was applied [11]. Zincian malachite (zM) was also the major phase in these ternary precursors related to industrial methanol synthesis catalysts $Cu/ZnO/Al_2O_3$, but its fraction decreased as the Al content increased above 6.5% due to the formation of hydrotalcite-like phase. Despite the fact that smaller Cu particles typically evolved from this new phase [12], they were encapsulated in large oxide aggregates, resulting in a lower methanol synthesis activity. Thus, the hydrotalcite (HT) was regarded as an undesired precursor phase in methanol synthesis [11]. To prevent the formation of this byproduct phase at higher Al concentrations, we recently applied sequential precipitation (SP) in which Al^{3+} was precipitated onto the fully aged Cu,Zn precipitate of zM phase [13]. The resulting $Al_2O_3/Cu/ZnO$ catalysts with the Al content of 13-40% enabled the direct production of dimethyl ether from syngas with yields that were two- to three-fold higher than those obtained with their co-precipitated counterparts. The SP-derived catalysts with 20-40% Al also showed higher methanol synthesis activity. However, when the Al content was 13%, the CP-derived catalyst was superior to the SP-derived analogue, even though zM and HT phases were both found in the precursor of the former, whereas only zM phase in the precursor of the latter. This may create a doubt on whether HT phase is an activity-unfavorable phase.

Thus, we have attempted to manipulate the relative fraction of HT to zM phase in a co-precipitated Cu,Zn,Al precursor. Our first attempt was to add a fourth metal component, Zr, into the ternary precursor by changing the concentration ratio of Al to Zr in the metal solution [14]. This approach was successful in the controlled formation of HT phase relative to zM phase in Cu,Zn,Al,Zr precursor, yet its exact effect on the catalytic activity was rather difficult to evaluate since the electronic character of ZrO_2 is different from that of Al_2O_3. As another approach, we paid attention to our SP method applied for Cu,Zn,Al precursors because only zM phase was produced even with higher Al content due to Al^{3+} precipitation onto the "fully aged" Cu,Zn precipitate. For the purpose of controlling the relative fraction of HT to zM phase, the time to inject Al^{3+} solution into a preformed Cu,Zn suspension was adjusted as employed in this study. The benefit of this strategy is to attain the identical metal composition of all Cu,Zn,Al precursors, if successful, though prepared in a different manner: the nominal metal composition Cu : Zn : Al was herein fixed at 63.7 : 27.3 : 9.0 (i.e., nominal Al content of 9%) because the reflections of HT phase were intense for the co-precipitated precursor of this Al content [14]. Therefore, our approach is helpful in elucidating the effect of HT phase on the methanol synthesis activity and specific copper sur-

†To whom correspondence should be addressed.
E-mail: ywsuh@hanyang.ac.kr
‡C. Jeong and J. Park contributed equally to this work.
‡Current address: Gwangyang Research Group, Research Institute of Industrial Science & Technology (RIST), Gwangyang 57801, Korea

face area. All prepared precursors were characterized by XRD and TG-MS measurements to distinguish the phases of HT and zM. Final $Cu/ZnO/Al_2O_3$ catalysts were tested in CO_2 hydrogenation to methanol.

EXPERIMENTAL

1. Catalyst Preparation

For sequential precipitation, the solution of 32.65 g $Cu(NO_3)_2 \cdot 3H_2O$ and 17.40 g $Zn(NO_3)_2 \cdot 6H_2O$ in 159.25 mL H_2O (nominal Cu/Zn=70 : 30) was added dropwise (14 cm^3 min^{-1}) into 0.12 M $NaHCO_3$ solution (4,200 mL) at 343 K under vigorous stirring. After ageing of Cu,Zn precipitate at 343 K for a desired period, Al^{3+} solution made up of 7.23 g $Al(NO_3)_3 \cdot 9H_2O$ in 15.75 mL H_2O was added at the rate of 14 cm^3 min^{-1}. Further ageing under stirring was conducted for (90−x) min. Therefore, the total ageing period was 90 min.

The prepared precursor with the nominal Al content of 9% was labeled as CZA-SP-x, where x represents the ageing time of Cu,Zn precipitate. The x value of 10, 30 or 60 was determined according to the pH drop of 0.03 unit observed at ca. 20 min after the start of ageing (Fig. 1). For CZA-SP-10, Al^{3+} was added before pH drop. CZA-SP-30 and CZA-SP-60 were obtained by addition of Al^{3+} just after pH drop and onto the fully aged Cu,Zn precipitate, respectively. The final pH values in all cases were in the similar pH range 6.30-6.44, which is above pH 5 to meet the minimum pH requirement for complete co-precipitation [15].

Co-precipitation was applied for binary Cu,Zn (CZ-CP) and ternary Cu,Zn,Al (CZA-CP) precursors with the nominal Cu/Zn of 70 : 30. First, an aqueous metal solution was prepared by dissolving 35.87 g $Cu(NO_3)_2 \cdot 3H_2O$ and 19.12 g $Zn(NO_3)_2 \cdot 6H_2O$ for CZ-CP or 32.65 g $Cu(NO_3)_2 \cdot 3H_2O$, 17.40 g $Zn(NO_3)_2 \cdot 6H_2O$, and 7.23 g $Al(NO_3)_3 \cdot 9H_2O$ for CZA-CP in 175 mL H_2O. This was added dropwise (14 cm^3 min^{-1}) into 0.12 M $NaHCO_3$ solution (4,200 mL) at 343 K under vigorous stirring. Then, the precipitate suspension was aged for 90 min.

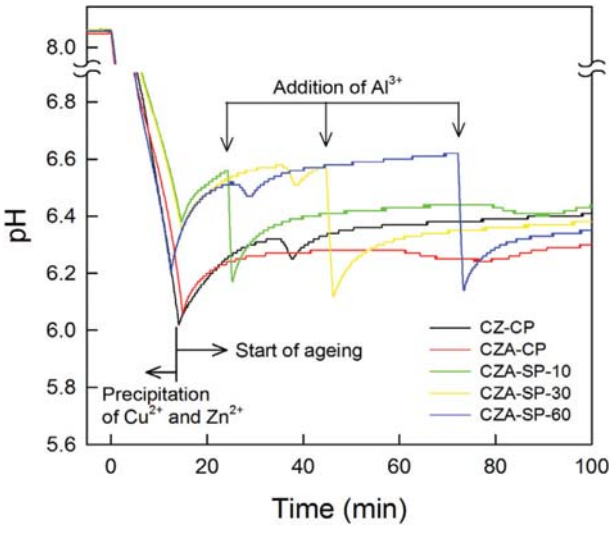

Fig. 1. Solution pH profiles monitored during precipitation and ageing for the precursors CZ-CP, CZA-CP, CZA-SP-x (x=10, 30 or 60).

The aged precipitate was thoroughly washed with deionized water at least four times, followed by drying in a convection oven at 378 K overnight. The dried precursor sample was calcined in a muffle furnace at 603 K (2 K min^{-1}) for 3 h. Prior to the activity test, Cu,Zn,Al-mixed oxide sample was pelletized, crushed, and then sieved to the size smaller than 200 μm.

2. Characterization

Powder X-ray diffraction (XRD) patterns were recorded on a Rigaku miniFlex600 diffractometer using a Cu Kα radiation source (40 kV and 15 mA). Thermogravimetric (TG) profiles were obtained in a NETZSCH TG209F1 coupled with a mass spectrometer, as the sample was heated to 1,073 K at 10 K min^{-1} in an air flow (100 cm^3 min^{-1}). For transmission electron microscopy (TEM) analysis, a JEOL JEM 2100F microscope was used with a Gatan Digital Micrograph imaging filter. The Brunauer-Emmett-Teller (BET) surface area (0.15 g sample) was measured in a Micromeritics ASAP 2020 after pretreatment at 373 K for 1 h under vacuum. The metal composition of mixed oxide samples was measured by inductively coupled plasma optical emission spectroscopy (ICP-OES) using an iCAP 7000 series (Thermo Fisher Scientific). Temperature-programmed reduction (TPR) experiment was conducted in a Micromeritics TPD/TPR 2900 instrument with a thermal conductivity detector. As the sample (50 mg) was heated at 2.5 K min^{-1} in a 10% H_2/Ar flow (50 cm^3 min^{-1}), the effluent gas was measured by using a mass spectrometer (Balzers Prisma QME 200).

For N_2O reactive frontal chromatography (N_2O-RFC) experiment, the sample (0.1 g) was reduced at 523 K for 1 h in a 10% H_2/Ar flow (30 cm^3 min^{-1}) in a BELCAT-B instrument with a BEL-Mass (BEL Japan, Inc.). After cooling to 313 K in He, 1% N_2O/He (5 cm^3 min^{-1}) was introduced while the emission of N_2 (m/z=28) in the effluent gas was quantitatively measured. The reaction stoichiometry Cu/O and copper surface density are two and 1.46×10^{19} Cu atom m^{-2}, respectively. Even if some reduced Zn species can be oxidized by N_2O [16,17], the measured copper surface area is still important in interpreting the catalytic performance of Cu/ZnO-based catalysts.

3. Activity Test

For methanol synthesis reaction, the mixed oxide sample (0.1 g) was reduced at 523 K for 3 h (1 K min^{-1}) using 20% H_2 in N_2 (100 cm^3 min^{-1}) in a stainless steel reactor. After cooling to 503 K, the reaction gas ($H_2/CO_2/N_2$/He=59.5 : 14 : 4 : balance, 100 cm^3 min^{-1}, GHSV 60,000 L kg_{cat}^{-1} h^{-1}) was fed and pressurized to 30 bar. This condition is similar to that reported by Schumann et al. [18,19]. The effluent gas was analyzed by an online Agilent 7890A GC system. In all reaction runs the conversion of CO_2 was below 4% due to a near-differential condition and other products except methanol and CO formed by reverse water gas shift reaction were not detected indicating negligible acidity of the prepared catalysts because the Al content of 9% in this work was lower than that of $Cu/ZnO/Al_2O_3$ employed in our previous report [13]. Also, the stability of all tested catalysts was similar (Fig. S1).

RESULTS AND DISCUSSION

In XRD patterns presented in Fig. 2, the (20−1) reflection of zM

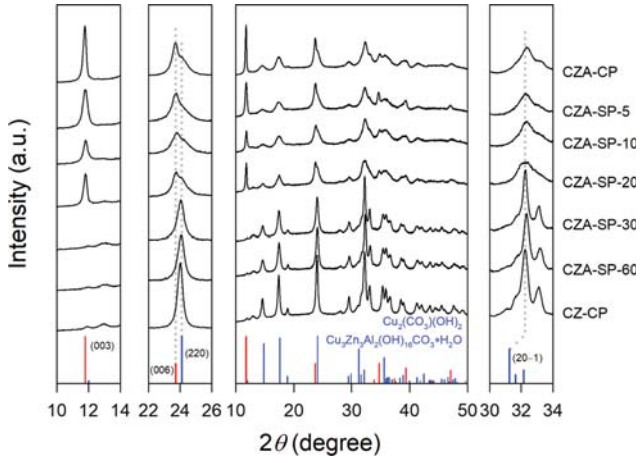

Fig. 2. XRD patterns of the precursors CZ-CP, CZA-CP, and CZA-SP-*x* (*x*=5, 10, 20, 30 or 60), where the 2θ ranges in 10-14°, 22-26°, and 30-34° are enlarged.

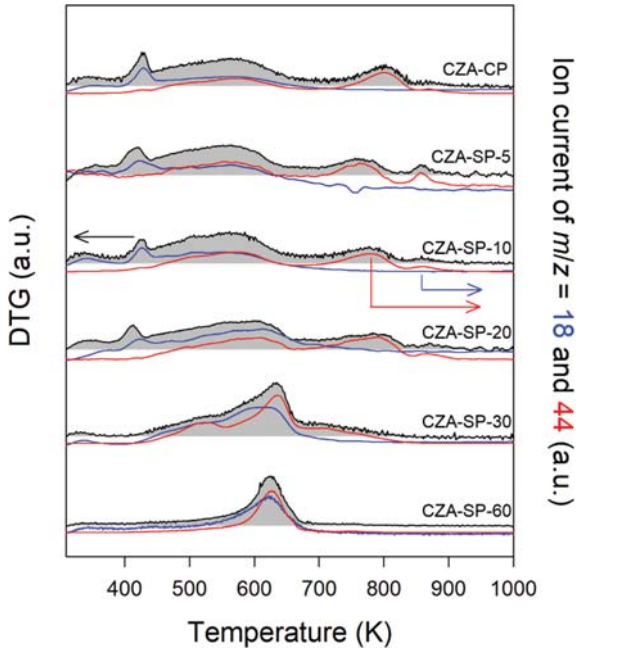

Fig. 3. TG derivative curves of the prepared precursors (black) and the corresponding mass fragments of *m*/*z*=18 (blue) and 44 (red) representing the emission of H_2O and CO_2.

phase around 2θ=32.37° and the (003) reflection of HT phase at 2θ=11.80° were first compared. Each of these reflections was clearly seen in XRD patterns of CZ-CP and CZA-CP, respectively. The (20−1) reflection for SP precursors was detected at the similar 2θ angle to that for CZ-CP, where the calculated *d*-spacing value was similar at 2.770-2.775 Å. This suggests that displacement of Cu^{2+} by Zn^{2+} is not largely affected by the SP method. According to the report of Behrens [9], these values correspond to the case that Zn occupancy of metal sites in zM structure is approximately of 30%. However, the (20−1) reflection for CZA-SP-10 was not sharp compared to that for CZA-SP-30 and CZA-SP-60. This is associated with HT phase because only CZA-SP-10 among three SP precursors showed the sharp (003) reflection of HT phase of which the intensity was equivalent to ca. one third of that for CZA-CP.

Additionally, the reflections around 2θ=24° were examined. For CZA-SP-30, CZA-SP-60, and CZ-CP, the reflections were centered at 2θ=24.10° corresponding to the (220) plane of zM phase, indicating that these precursors consist of relatively pure zM phase. However, CZA-CP and CZA-SP-10 showed the major reflection at 2θ=23.71°, representing the (006) plane of HT phase, with a shoulder at 2θ=24.10°. This means that the two precursors are made up of a mixture of zM and HT phases. When calculated using the intensities of two reflections, the fraction of HT phase was 64% and 58% for CZA-CP and CZA-SP-10, respectively, i.e., HT phase was less abundant in CZA-SP-10.

These XRD results are consistent with the findings by TG-MS analysis (Fig. 3). CZA-SP-30 and CZA-SP-60 were decomposed at 473-673 K (dehydroxylation and decarbonylation) and at 673-843 K (complete decarbonylation), indicating that these precursors were of pure zM phase [20]. In contrast, CZA-SP-10 and CZA-CP showed decomposition events at <473 K (dehydroxylation of brucitic layers), 473-673 K (minor dehydroxylation and decarbonylation), and 673-900 K (complete decarbonylation), which is typically observed in HT-containing materials [12]. Although the DTG curve of CZA-SP-10 looked similar to that of CZA-CP, the peak at 473-673 K was slightly higher and the peak at 673-900 K was less and shifted to a low temperature for CZA-SP-10. This is also explained by the fact that HT phase was less abundant in CZA-SP-10 than in CZA-CP.

Additionally, the precursors CZA-SP-5 and CZA-SP-20 were prepared by adding the Al solution at 5 and 20 min after the start of ageing, respectively, and characterized by XRD and TG-MS analysis. Figs. 3 and 4 clearly show that these precursors resemble CZA-SP-10, indicating that they are also composed of a mixture of zM and HT phases. The calculated fraction of HT phase was 60% and 54% for CZA-SP-5 and CZA-SP-20, respectively. This suggests that the fraction of HT phase becomes deficient as the addition of Al^{3+} solution before pH drop is to be late. Since CZA-SP-10 is an interim precursor between CZA-SP-5 and CZA-SP-20, a calcined form of the former precursor was used to compare XRD, TPR and TEM characteristics of Cu,Zn,Al-mixed oxide samples.

Therefore, the evolution of HT phase was controlled by tuning the time to inject Al^{3+} solution. When Al^{3+} was added after pH drop, its incorporation into crystalline Cu,Zn precipitate was very hard, hence zM phase being dominant in the precursor. However, the addition of Al^{3+} before pH drop enabled some fraction of Al^{3+} ion to interact with divalent Cu and Zn ions of primitive Cu,Zn precipitate, resulting in the formation of HT phase in less abundance compared to CZA-CP prepared by co-precipitation. Note that the fraction of Al^{3+} non-incorporated into HT phase would be precipitated independently or onto the external surface of Cu,Zn precipitate.

Fig. 4 shows the major reflections of CuO with minor reflections of ZnO in XRD patterns of Cu,Zn,Al-mixed oxide samples. The calculation using the (−111) reflection of CuO at 2θ=35.55° revealed that the crystallite size of CuO decreased in the following order: CZA-SP-60 (4.9±0.1 nm)>CZA-SP-30 (4.2±0.1 nm)>CZA-SP-10 (3.8±0.2 nm). Note that the Cu/Zn/Al composition in all mixed oxide samples was estimated to be similar around 65.2-

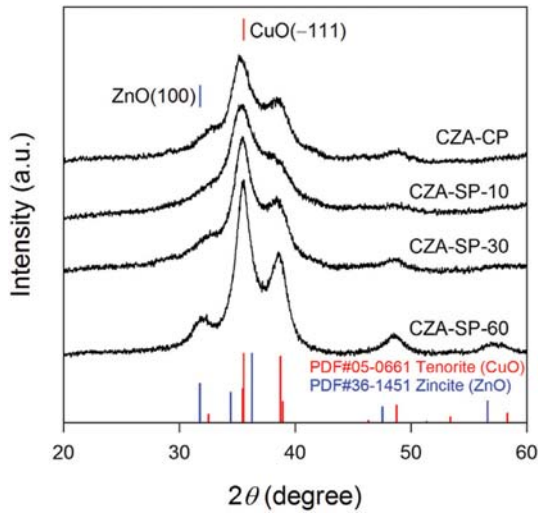

Fig. 4. XRD patterns of Cu, Zn, Al-mixed oxide samples, where the standard reflections of tenorite (CuO) and zincite (ZnO) are included at the bottom.

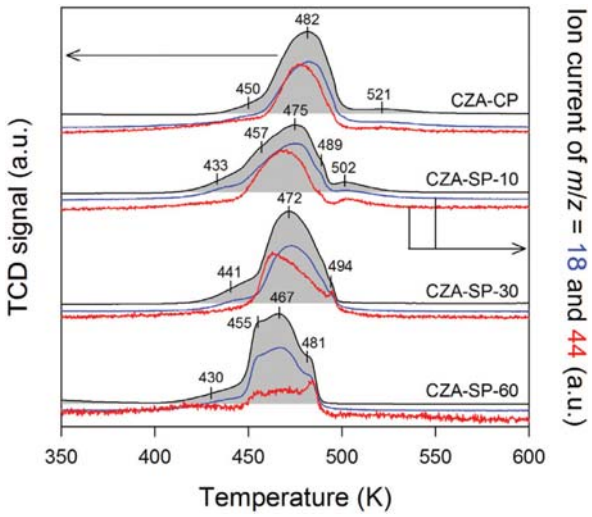

Fig. 5. H_2 consumption profiles (black) of Cu, Zn, Al-mixed oxide samples, accompanied by the emission of mass fragments of m/z=18 (blue) and 44 (red).

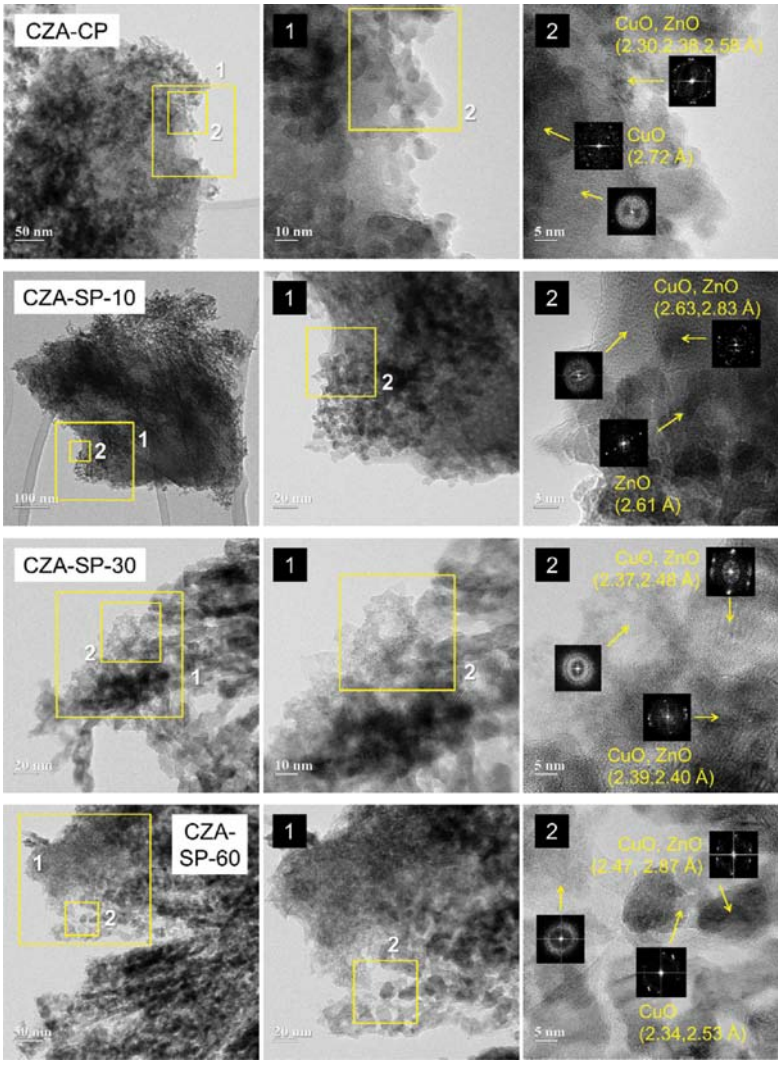

Fig. 6. TEM images of Cu, Zn, Al-mixed oxide samples. Right two images in each line are the magnified version of rectangular areas in the left image. The insets show electron diffraction patterns of local areas that are used for calculating the *d*-spacing value of CuO or ZnO.

66.0 : 26.0-26.3 : 8.1-8.5. A similar trend appeared in the (100) reflection of ZnO at 2θ=31.77°, though not calculated actually due to peak overlapping. Interestingly, CZA-CP showed somewhat higher reflections of CuO and ZnO than CZA-SP-10, where the calculated CuO size in CZA-CP was 4.1±0.1 nm.

The reduction characteristic of Cu,Zn,Al-mixed oxide samples was investigated by TPR-MS experiment (Fig. 5). In H_2 consumption of CZA-CP, the peak above 500 K was ascribed to the reduction of Cu^{2+} ion embedded within amorphous Zn-Al oxide matrix derived from HT phase, accompanied by CO_2 emission [12]. A similar peak was found at 502 K in H_2 consumption of CZA-SP-10. Additionally, CZA-SP-10 exhibited broad H_2 consumption in 430-500 K, where the major peak was centered at 475 K with weak shoulders at 433, 457, and 489 K. Similar reduction features were seen for CZA-SP-30 and CZA-SP-60, although a small shift was observed.

The nanostructure of Cu,Zn,Al-mixed oxide samples was visualized by TEM analysis (Fig. 6). In the low magnification images of CZA-SP-30 and CZA-SP-60 was observed the needle-type morphology reported for CuO/ZnO derived from zM phase [9]. Moreover, some granular particles of crystalline CuO and ZnO (identified by electron diffraction patterns) were surrounded by amorphous particles of Al rich. This is a result of Al^{3+} precipitation onto the aged Cu,Zn precipitate [13]. On the other hand, some of CuO and ZnO particles appeared to be covered by amorphous layers for CZA-CP and CZA-SP-10, which is characteristic of Cu,Zn,Al-mixed oxide derived from HT phase [12]. However, the difference was not distinguishable in the high magnification images of two samples.

Thus, the Cu surface area (SA_{Cu}) of reduced catalysts was measured by N_2O-RFC experiment. The SA_{Cu} value increased in the following order: CZA-SP-60 (28.3 $m^2\ g^{-1}$)<CZA-SP-30 (32.1 $m^2\ g^{-1}$)< CZA-SP-20 (36.6 $m^2\ g^{-1}$)<CZA-CP (38.4 $m^2\ g^{-1}$)<CZA-SP-5 (39.1 $m^2\ g^{-1}$)≈CZA-SP-10 (39.7 $m^2\ g^{-1}$). That is, the accessible Cu surface was the largest for CZA-SP-5 and CZA-SP-10. A similar trend was obtained in the methanol productivity (Fig. 7): CZA-SP-60 (327.0±16.3 g $kg_{cat}^{-1}\ h^{-1}$)<CZA-SP-30 (354.6±18.9 g $kg_{cat}^{-1}\ h^{-1}$)< CZA-SP-20 (363.5±14.2 g $kg_{cat}^{-1}\ h^{-1}$)<CZA-CP (368.8±22.3 g $kg_{cat}^{-1}\ h^{-1}$)<CZA-SP-10 (395.3±26.0 g $kg_{cat}^{-1}\ h^{-1}$)≈CZA-SP-5 (401.1±9.6 g $kg_{cat}^{-1}\ h^{-1}$). Notably, the superior activity of CZA-CP to CZA-SP-60 is compatible with the activity difference observed when the Al^{3+} content was 13% [13]. In further tests under a different reaction condition ($H_2/CO_2/N_2$=72 : 24 : 4, 503 K, 30 bar, GHSV 15,000 L $kg_{cat}^{-1}\ h^{-1}$), CZA-SP-5 and CZA-SP-10 also showed better performance than the other catalysts (not shown for the sake of brevity).

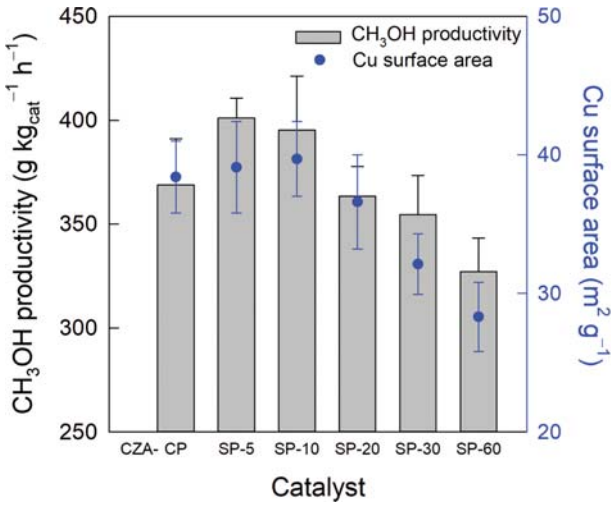

Fig. 7. Methanol synthesis activities and Cu surface areas of $Cu/ZnO/Al_2O_3$ catalysts prepared in this work. Reaction condition: 503 K, 30 bar, $H_2/CO_2/N_2/He$=59.5 : 14 : 4 : balance, GHSV 60,000 L $kg_{cat}^{-1}\ h^{-1}$.

In case of CZA-SP-30 and CZA-SP-60, Al^{3+} was not incorporated into crystalline Cu,Zn precipitate of zM phase, thus Al_2O_3 being separate from Cu/ZnO particles in the reduced catalyst. Therefore, the low SA_{Cu} values and methanol productivities of these catalysts are possibly a result of blocking accessible Cu surface by Al_2O_3 particles and less Al promotion to Cu/ZnO particles. In contrast, HT phase along with zM phase was present in the precursors CZA-CP, CZA-SP-5, CZA-SP-10 and CZA-SP-20. Since Cu^{2+} and Zn^{2+} are mixed with Al^{3+} in HT phase, Al promotion is likely to exist in their final catalysts. However, when HT phase is much present in the precursor, CuO and Cu particles are embedded within amorphous Zn-Al oxide matrix after calcination and reduction, respectively. This explains a little lower Cu surface area and methanol synthesis activity of CZA-CP compared to CZA-SP-5 and CZA-SP-10 of which the precursor contained HT phase in less abundance. On the contrary, a slightly lower catalytic performance of CZA-SP-20 than CZA-CP is considered to result from less Al promotion because the calculated fraction of HT phase was smaller by 10% for the former precursor than for the latter.

Finally, the catalytic performance of CZA-SP-10 was compared with that of $Cu/ZnO/ZrO_2/Al_2O_3$ catalysts with the similar Al content in our recent report, that is, 9Al+1Zr (Q5), 9Al+7Zr (Q6), 9Al+9Zr (Q7) and 9Al+21Zr (Q8) [14]. The methanol productivity of these catalysts was in the range 409-425 g $kg_{cat}^{-1}\ h^{-1}$ that was higher than the activity of CZA-SP-10 (395.3±26.0 g $kg_{cat}^{-1}\ h^{-1}$). Although the approach chosen in this study may be underestimated due to this result, it should be noted that the interaction between Cu and ZrO_2 strongly affects the hydrogenation of formate species and hydrogen spillover [21], explaining the superior performance of the above quaternary catalysts.

CONCLUSION

We investigated the effect of sequential precipitation conducted in such a manner that Al^{3+} solution is added into the pre-formed Cu,Zn precipitate. The precipitation of Al^{3+} after crystallization of Cu,Zn precipitate had a negative effect on the methanol synthesis activity because Al_2O_3 particles are located at the external surface of Cu/ZnO particles, hindering the access to active Cu surface. However, Al^{3+} precipitation onto primitive, amorphous Cu,Zn precipitate brought about the improvement in Cu surface area and catalytic performance. Although the precursor prepared in this fashion was a mixture of zM and HT phases like the co-precipitated precursor, HT phase was less abundant due to insufficient mixing of Al^{3+} with Cu^{2+} and Zn^{2+}, which affected the accessibility of Cu particles. Even though the activity enhancement was not huge in this work, the attempt to tune the phase of Cu,Zn,Al precursor is

worth being studied consistently.

ACKNOWLEDGEMENTS

This work was supported by "Next Generation Carbon Upcycling Program (NRF-2017M1A2A2043148)" through the National Research Foundation (NRF) funded by the Ministry of Science and ICT, and by "Basic Science Research Program (NRF-2016R1A6A1 A03013422)" through the NRF funded by the Ministry of Education, Republic of Korea. We also acknowledge the financial support from the Korea Institute of Energy Technology Evaluation and Planning under the Ministry of Trade, Industry and Energy, Republic of Korea (KETEP-20163010092210).

SUPPORTING INFORMATION

Additional information as noted in the text. This information is available via the Internet at http://www.springer.com/chemistry/journal/11814.

REFERENCES

1. C. Jeong and Y.-W. Suh, *Appl. Chem. Eng.*, **27**, 555 (2016).
2. N.-K. Park and T. J. Lee, *Korean J. Chem. Eng.*, **28**(10), 2076 (2011).
3. D.-L. Vu and J.-W. Lee, *Korean J. Chem. Eng.*, **33**(2), 514 (2016).
4. E. G. Choi, K. H. Song, K. Y. Lee, M. H. Youn, K. T. Park, S. K. Jeong and H. J. Kim, *Korean J. Chem. Eng.*, **35**(1), 73 (2018).
5. W. Li, P. Lu, D. Xu and K. Tao, *Korean J. Chem. Eng.*, **35**(1), 110 (2018).
6. S. Schimpf and M. Muhler, Methanol catalysts, in: K. P. de Jong (Ed.), Synthesis of Solid Catalysts, Wiley-VCH, Weinheim, 329 (2009).
7. D. M. Whittle, A. A. Mirzaei, J. S. J. Hargreaves, R. W. Joyner, C. J. Kiely, S. H. Taylor and G. J. Hutchings, *Phys. Chem. Chem. Phys.*, **4**, 5915 (2002).
8. B. Bems, M. Schur, A. Dassenoy, H. Junkes, D. Herein and R. Schlögl, *Chem. Eur. J.*, **9**, 2039 (2003).
9. M. Behrens, *J. Catal.*, **267**, 24 (2009).
10. S. Zander, B. Seidlhofer and M. Behrens, *Dalton Trans.*, **41**, 13413 (2012).
11. M. Behrens, S. Zander, P. Kurr, N. Jacobsen, J. Senker, G. Koch, T. Ressler, R. W. Fischer and R. Schlögl, *J. Am. Chem. Soc.*, **135**, 6061 (2013).
12. M. Behrens, I. Kasatkin, S. Kühl and G. Weinberg, *Chem. Mater.*, **22**, 386 (2010).
13. C. Jeong, H. Ham, J. W. Bae, D.-C. Kang, C.-H. Shin, J. H. Baik and Y.-W. Suh, *ChemCatChem*, **9**, 4484 (2017).
14. J. Kim, C. Jeong, J. H. Baik and Y.-W. Suh, *Catal. Today*, in press (2018). DOI:10.1016/j.cattod.2018.09.008.
15. M. Behrens, D. Brennecke, F. Girgsdies, S. Kißner, A. Trunschke, N. Nasrudin, S. Zakaria, N. F. Idris, S. B. A. Hamid, B. Kniep, R. Fischer, W. Busser, M. Muhler and R. Schlögl, *Appl. Catal. A.*, **392**, 93 (2011).
16. M. B. Fichtl, J. Schumann, I. Kasatkin, N. Jacobsen, M. Behrens, R. Schlögl, M. Muhler and O. Hinrichsen, *Angew. Chem. Int. Ed.*, **53**, 7043 (2014).
17. S. Kuld, C. Conradsen, P. G. Moses, I. Chorkendorff and J. Sehested, *Angew. Chem. Int. Ed.*, **53**, 5941 (2014).
18. J. Schumann, T. Lunkenbein, A. Tarasov, N. Thomas, R. Schlögl and M. Behrens, *ChemCatChem*, **6**, 2889 (2014).
19. J. Schumann, M. Eichelbaum, T. Lunkenbein, N. Thomas, M. C. Á. Galván, R. Schlögl and M. Behrens, *ACS Catal.*, **5**, 3260 (2015).
20. M. Behrens, F. Girgsdies, A. Trunschke and R. Schlögl, *Eur. J. Inorg. Chem.*, 1347 (2009).
21. Y. H. Wang, W. G. Gao, H. Wang, Y. E. Zheng, W. Na and K. Z. Li, *RSC Adv.*, **7**, 8709 (2017).

Supporting Information

Effects of Al^{3+} precipitation onto primitive amorphous Cu-Zn precipitate on methanol synthesis over $Cu/ZnO/Al_2O_3$ catalyst

Cheonwoo Jeong[*,‡,‡], Jongha Park[*,‡], Jinsung Kim[*], Joon Hyun Baik[**], and Young-Woong Suh[*,*,†]**

*Department of Chemical Engineering, Hanyang University, Seoul 04763, Korea
**Energy Research Group, Research Institute of Industrial Science & Technology, Pohang 37673, Korea
***Research Institute of Industrial Science, Hanyang University, Seoul 04763, Korea
(*Received 20 June 2018 • accepted 3 November 2018*)

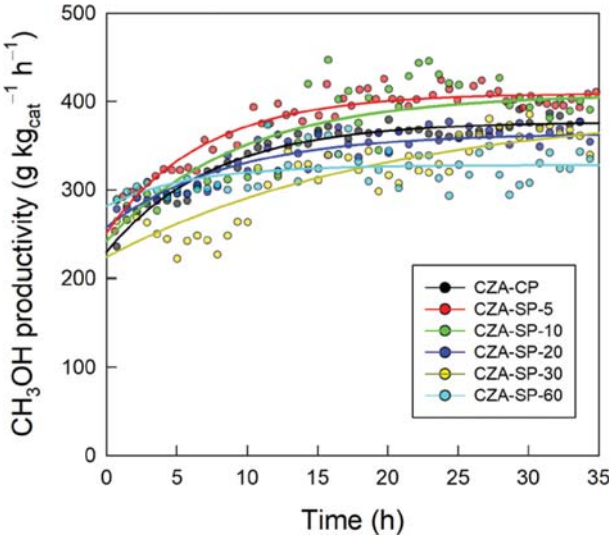

Fig. S1. Methanol productivity as a function of time on stream over the catalysts tested in this work. Reaction condition: 503 K, 30 bar, $H_2/CO_2/N_2$/He=59.5 : 14 : 4 : balance, GHSV 60,000 L kg_{cat}^{-1} h^{-1}).